A thermodynamic explanation for black smoker temperatures

Tim Jupp & Adam Schultz

Institute of Theoretical Geophysics, Department of Earth Sciences, University of Cambridge, Cambridge CB2 3EQ, UK

There is a remarkable difference between the maximum temperature of black smoker effluent (350°C - 400°C) and the temperature of the solidifying magma which heats it (~1200°C)[1,2,3]. For some time, it has been suspected[4] that the nonlinear thermodynamic properties of water[5] might be responsible. Here, we transform this hypothesis into a physical model by examining the internal temperature structure of convection cells in a porous medium. At pressures appropriate to seafloor crust, we demonstrate that pure water plumes naturally form at ~400°C for any sufficient heat source. Higher temperatures (>~500°C) are confined to a boundary layer at the base of the cell, where flow is horizontal. The phenomenon is explained analytically using the thermodynamic properties of water, and is illustrated by numerical simulations. Our model predicts the existence of the high temperature 'reaction zone' found in ophiolites[6], and suggests that vent temperatures will remain steady as magma chambers solidify and cool[7].

Three mechanisms to limit black smoker temperatures have been proposed. The first suggestion is that high temperature rock (say, >500°C) is effectively impermeable, because its ductile nature prevents the formation of cracks[8,9]. The second is that high temperature rock becomes impermeable over time, either by mineral precipitation[4,10], or by thermal expansion of the rock[11]. The third hypothesis is that the temperature cap is imposed by the thermodynamic properties of water. The first two models work by restricting flow to sufficiently cool regions of the crust. In contrast, the third model allows fluid to flow at all temperatures within the crust but limits the temperature of the fluid expelled at the seafloor.

Previous studies have shown how the thermodynamic properties of water affect the onset of convection[12] and the overall rate of heat transfer in convection cells operating across a small temperature difference (~10°C)[13,14]. Given a fixed temperature difference, cells operating near the critical point of water (~22 MPa, ~374°C) transfer heat much more rapidly than cells at other temperatures. Such 'superconvection' suggests that hydrothermal systems should be effective at heat transfer, but it is insufficient to explain the limit to vent temperatures. Real systems operate between ~10°C and ~1200°C - a large temperature difference - and vent at a particular temperature (~400°C). To explain this, the focus of investigation must move from the overall heat transfer to the internal temperature structure of the cell.

A numerical simulation can be used to illustrate the thermal structure of convection cells[15] (Fig.1). This simulation uses parameter values appropriate to seafloor systems. However, analysis of the governing equations shows that the key feature of the temperature structure depends solely on the thermodynamics of water, and not on the details of the parametrisation. To isolate the phenomenon under discussion, all previously suggested temperature-limiting mechanisms are excluded, and the crust is taken to be homogeneous and isotropic. Simulations were performed with the package HYDROTHERM[16] (available at http://water.usgs.gov/software/hydrotherm.html), modified to enforce a thermal boundary condition relevant to seafloor systems[17]. (Hot effluent emerges from an otherwise cold seafloor, so a fixed temperature boundary condition is not always appropriate. Consequently, the condition $\partial T/\partial z=0$ is imposed on the seafloor where flow is upwards, and T=10ºC is imposed where flow is downwards).

The governing equations are Darcy's law[18], an equation of state for pure wate[19,20,21,22], and the conservation of mass and energy in a porous medium[18]. Convection is initiated by a 'heater' along part of the bottom boundary[23], which represents the top of a magma chamber. For simplicity, the heater imposes a Gaussian (bell-shaped) temperature profile which runs from

'cold' (T_0) at the sides to 'hot' ($T_0+\Delta T$) at the centre. The heater is 'switched on' at time zero, when the domain is cold ($T=T_0$) and at hydrostatic pressure. Time-dependent solutions for the temperature and pressure fields are calculated and allowed to evolve until a steady state is reached.

A typical steady solution with T_0=10°C and ($T_0+\Delta T$)=1200°C is shown in Fig. 1. There is a thin boundary layer of very hot fluid (500°C to 1200°C) at the base of the convection cell. This layer, in which flow is horizontal, can be compared with the 'reaction zone' observed in ophiolites, for which similar temperatures have been inferred[6]. The temperature of the plume is about 400°C. Similar plume temperatures were obtained for other convectively-dominated systems with T_0=10°C and ($T_0+\Delta T$)>~500°C, including systems with anisotropic permeability. It follows that vent temperatures could remain steady as a magma chamber solidified and cooled, dropping only when the heat source fell below ~500°C.

It appears that plumes have a natural tendency to form at ~400°C, given a sufficient heat source and seafloor pressures. The explanation for this phenomenon lies in the balance between conduction and advection - the two mechanisms which transport energy in a convection cell.

In the model (Fig. 1), the temperature T and pressure p are functions of position $\mathbf{x}=(x,z)$. Thermal gradients produce a conductive heat flux $-\lambda\nabla T$, where λ is the thermal conductivity. Fluid motion creates an advective heat flux $\rho h\mathbf{u}$, for water of density ρ, specific enthalpy h and Darcy velocity $\mathbf{u}$. In the conservation of energy equation[18], the rate of change of energy per unit volume is given by the negative divergence of the total heat flux, or $-\nabla\cdot(\rho h\mathbf{u}-\lambda\nabla T)$. This can be split into two terms, $-\nabla\cdot(\rho h\mathbf{u})$ and $\lambda\nabla^2 T$, which are rates of accumulation of energy per unit volume, due to advection and conduction respectively. At any point in the cell, the relative importance of these two mechanisms can be expressed by the ratio $Ra_L(\mathbf{x},t)=\left|\nabla\cdot(\rho h\mathbf{u})/\lambda\nabla^2 T\right|$. This ratio measures the influence of fluid motion on the evolution

of the local temperature field, and could logically be labelled the 'local Rayleigh number'. (Traditionally, a single parameter - the 'Rayleigh number' - is defined for the whole cell[12]. Here, a 'local Rayleigh number' has been assigned, independently, to each point in the cell.) If $Ra_L \ll 1$, conduction dominates over advection, and the temperature evolves independently of any fluid flow. Conversely, where $Ra_L \gg 1$, advection is strong enough to influence the temperature field, and the isotherms can be distorted away from a conductively-dominated pattern. Advective distortion of the isotherms marks the separation of the plume from the boundary layer – indeed, it is what defines the plume on a plot of the temperature field (Fig. 1). To discover where plumes will appear, it is important to know where Ra_L is largest.

After the heater is switched on, a thermal signal propagates upwards (Fig. 2). For the period before plume formation (Fig. 2a,b), the approximate magnitudes of the energy accumulation terms can be calculated. Let d be the distance that the signal has penetrated into the domain, that is, the vertical range over which the temperature drops from 'hot' ($T_0+\Delta T$) to 'cold' (T_0). Suppose that $\left|\rho h \mathbf{u}\right|$ is of order Φ. Hence $\left|\nabla\cdot(\rho h \mathbf{u})\right|$ is of order Φ/d, while $\left|\lambda \nabla^2 T\right|$ is of order $\lambda\Delta T/d^2$. Consequently, Ra_L is of order $(\Phi/\lambda\Delta T)\cdot d$, and so scales linearly with the vertical length scale d. Just before plume formation, d is sufficiently small that Ra_L is everywhere of order unity (Fig. 2a). Note that Ra_L is greatest near the 400°C isotherm. A short time later, when d, and hence Ra_L, have increased slightly, plumes appear at about 400°C (Fig. 2c).

By making some simplifications, it is possible to estimate the temperature at which Ra_L is maximised, just before plume formation. Temperature gradients are nearly uniform (Fig. 2b). It follows that the maximum value of Ra_L is controlled by the maximum value of $\left|\nabla\cdot(\rho h \mathbf{u})\right|$. By analogy with convection in a U-shaped pipe[24], a convection cell can be divided into a cold 'downflow limb' and a hot 'upflow limb'. The vertical pressure gradient must be sufficiently small for cold water to flow down the downflow limb, and sufficiently large for hot water to flow up the upflow limb. Hence, the pressure gradient lies between hot hydrostatic and cold

hydrostatic. The permeability is the same in both limbs, but the total resistance to flow is much greater in the upflow limb because of its smaller cross-sectional area (Fig. 1). It follows that the pressure gradient will be much closer to cold hydrostatic than hot hydrostatic. Hence $\partial p/\partial z \approx -\rho_0 g$, where ρ_0 is the density of cold water. Suppose that the advective heat flux $\rho h\mathbf{u}$ is dominated by its vertical component, which by Darcy's law[18] is $-k(\partial p/\partial z+\rho g)\rho h/\mu$, for permeability k, gravitational acceleration g, and dynamic viscosity μ. An approximate expression for the advective energy accumulation is then: $-\nabla\cdot(\rho h\mathbf{u}) \approx \left[\frac{\partial}{\partial z}\left(\frac{(\rho_0-\rho)\rho h}{\mu}\right)\right]\cdot[-gk]$

Denoting $(\rho_0-\rho)\rho h/\mu$ by F, it follows that Ra_L should be maximised where $|\partial F/\partial z|$ is maximised. The quantity F has been termed 'fluxibility'[1] and measures the ability of buoyancy-driven water to transport energy. Fluxibility is a function of the thermodynamic state of the water (ρ_0 is constant and ρ, μ and h are known as functions of pressure and temperature from steam tables[19,20,21,22]). Fig. 3a shows how fluxibility depends on pressure and temperature over an appropriate range. Clearly, in a seafloor hydrothermal system, the fluxibility varies greatly with temperature, but little with pressure. Before the formation of a plume, temperature is approximately a linear function of height (Fig. 2b). Thus, $|\partial F/\partial z|$ should be maximised roughly where $|\partial F/\partial T|$ is maximised.

Fig. 3c shows clear peaks in $|\partial F/\partial T|$ at ~384°C (p=25 MPa) and ~412°C (p=35 MPa). These are the temperatures at which plumes would separate from the boundary layer under the simplifying assumptions. They are remarkably close to the plume temperatures in the numerical simulation (Fig. 1a,1b,2c).

This analysis uses the properties of pure water, because values of ρ, μ and h are not available for salt water over all of the required temperature range[4,25]. When such data become available, the calculation should be repeated for salt water. It seems likely[4] that the peaks in the $|\partial F/\partial T|$ curves would be shifted to higher temperatures by about 30ºC. Nonetheless, the use of pure water has one definite advantage. At pressures greater than 22 MPa (seafloor

depth ~2.2 km), pure water is a single-phase fluid. Hence, the complication of phase separation has been removed from this analysis, and it has been possible to demonstrate a temperature-limiting mechanism which is independent of 'phase-separation' or 'two-phase effects'.

Three differences between this approach and classical studies of porous medium convection[26] should be noted. Firstly, convection is not here generated by a *uniformly* heated lower boundary. The presence of both 'hot' and 'cold' at the base of the cell ensures that there is always a horizontal temperature gradient and associated fluid flow. The point of interest is not the onset of convective motion, but the onset of convective distortion of the temperature field. Secondly, no use is made of the Boussinesq approximation[27], under which the advective heat flux would be simplified to $\rho_0 h\mathbf{u}$. The true value $\rho h\mathbf{u}$ is used here because ρ can vary from ρ_0 by a factor of 25. Thirdly, this analysis abandons the traditional Rayleigh number[27], which is an *overall* balance between advection and conduction, in favour of a *local* Rayleigh number giving the balance at each point in the cell. This permits a discussion of the precise position (equivalently, temperature) at which plumes form.

At a given pressure, and given a sufficient source of heat, a plume is likely to form at the temperature of maximum fluxibility gradient (Fig. 3c). Hence, if ambient pressures are known, plume formation temperatures could be inferred for single-phase hydrothermal systems. Vents may be cooler than this plume formation temperature because of conductive losses from the ascending fluid, but they cannot be hotter.

References

1 Lister, C.R.B. Heat transfer between magmas and hydrothermal systems, or, six lemmas in search of a theorem, *Geophys. J. Int.* **120**, 45-59 (1995).

2 Lowell, R.P., Rona, P.A. & Von Herzen, R.P., Seafloor hydrothermal systems, *J. Geophys. Res.* **100,** 327-352 (1995).

3 Wilcock, W.S.D., Cellular convection models of mid-ocean ridge hydrothermal circulation and the temperatures of black smoker fluids, *J. Geophys. Res.* **103**, 2585-2596 (1998).

4 Bischoff, J.L. & Rosenbauer, R.J., An empirical equation of state for hydrothermal seawater (3.2 percent NaCl), *Amer. J. Sci.* **285**, 725-763 (1985).

5 Johnson, J.W. & Norton, D., Critical phenomena in hydrothermal systems: state, thermodynamic, electrostatic, and transport properties of H_2O in the critical region, *Am. J. Sci.*, **291**, 541 – 648 (1991).

6 Gillis, K.M. & Roberts, M.D., Cracking at the magma-hydrothermal transition: evidence from the Troodos Ophiolite, Cyprus, *Earth Planet. Sci. Lett.* **169,** 227-244 (1999).

7 Lowell, R.P. & Germanovich, L.N., On the temporal evolution of high-temperature hydrothermal systems at ocean ridge crests, *J. Geophys. Res.* **99,** 565-575 (1994).

8 Lister, C.R.B., On the penetration of water into hot rock, *Geophys. J. R. Astr. Soc.* **39**, 465-509 (1974).

9 Fournier, R.O., The transition from hydrostatic to greater than hydrostatic fluid pressure in presently active continental hydrothermal systems in crystalline rock, *Geophys. Res. Lett.* **18,** 955-958 (1991).

10 Lowell, R.P., Van Cappellen, P. & Germanovich, L., Silica precipitation in fractures and the evolution of permeability in hydrothermal upflow zones, *Science* **260,** 192-194 (1993).

11 Germanovich, L.N. & Lowell, R.P., Percolation theory, thermoelasticity, and discrete hydrothermal venting in the Earth's crust, *Science* **255**, 1564-1567 (1992).

12 Straus, J.M. & Schubert, G., Thermal convection of water in a porous medium: effects of temperature- and pressure-dependent thermodynamic and transport properties, *J. Geophys. Res.* **82**, 325 – 333 (1977).

13 Dunn, J.C. & Hardee, H.C., Superconvecting geothermal zones, *J. Volcanol. Geotherm. Res.* **11,** 189-201 (1981).

14 Ingebritsen, S.E. & Hayba, D.O., Fluid flow and heat transport near the critical point of H_2O, *Geophys. Res. Lett.* **21,** 2199-2202 (1994).

15 Norton, D. & Knight, J., Transport phenomena in hydrothermal systems: cooling plutons, *Am. J. Sci.* **277**, 937 – 981 (1977).

16 Hayba, D.O. & Ingebritsen, S.E., The computer model HYDROTHERM, a three-dimensional finite-difference model to simulate ground-water flow and heat transport in the temperature range of 0 to 1,200 degrees Celsius, *U.S. Geological Survey Water-Resources Investigations Report* **94-4045,** (1994).

17 Dickson, P., Schultz, A., Woods, A., Preliminary modelling of hydrothermal circulation within mid-ocean ridge sulphide structures, in *"Hydrothermal Vents and Processes"*, (ed. Parson, L.M. et al.), *Geological Society Special Publication* **87**, 145-157 (1995).

18 Faust, C.R. & Mercer, J.W., Geothermal Reservoir Simulation 1. Mathematical Models for Liquid- and Vapor-Dominated Hydrothermal Systems, *Water Resources Res.* **15,** 23-30 (1979).

19 Haar, L., Gallagher, J.S. & Kell, G.S., *NBS/NRC Steam Tables,* 320pp. (Hemisphere, New York, 1984).

20 Watson, J.T.R., Basu, R.S. & Sengers, J.V., An improved representative equation for the dynamic viscosity of water substance, *J. Phys. Chem. Ref. Data* **9,** 1255-1290 (1980).

21 Sengers, J.V. & Kamgar-Parsi, B., Representative equations for the viscosity of water substance, *J. Phys. Chem. Ref. Data* **13,** 185-205 (1984).

22 Sengers, J.V. & Watson J.T.R., Improved international formulation for the viscosity and thermal conductivity of water substance, *J. Phys. Chem. Ref. Data* **15,** 1291-1314 (1986).

23 Elder, J.E., *Geothermal Systems* pp. 180 – 187 (Academic Press, London, 1981).

24 Pascoe, A.R. & Cann, J.R., Modelling diffuse hydrothermal flow in black smoker vent fields, in *"Hydrothermal Vents and Processes"*, (ed. Parson, L.M. et al.), *Geological Society Special Publication* **87,** 159 -173 (1995).

25 Anderko, A. & Pitzer, K.S., Equation-of-state representation of phase equilibria and volumetric properties of the system NaCl-H_2O above 573 K, *Geochim. et Cosmochim. Acta.* **57,** 1657-1680 (1993).

26 Lapwood, E.R., Convection of a fluid in a porous medium, *Proc. Cam. Phil. Soc.* **44,** 508-521 (1948).

27 Phillips, O.M., *Flow and reactions in permeable rocks* pp. 245-264 (Cambridge University Press, Cambridge, 1991).

Acknowledgements: We thank USGS for permission to use HYDROTHERM. The calculations reported here were carried out on the Enigma high-performance computing centre at the Institute of Theoretical Geophysics. The authors acknowledge the support of that facility by the Higher Education Research Foundation for England. T.E.J. is supported by a studentship from the Natural Environment Research Council. Correspondence and requests for materials should be addressed to T.E.J. (e-mail: tim@itg.cam.ac.uk).

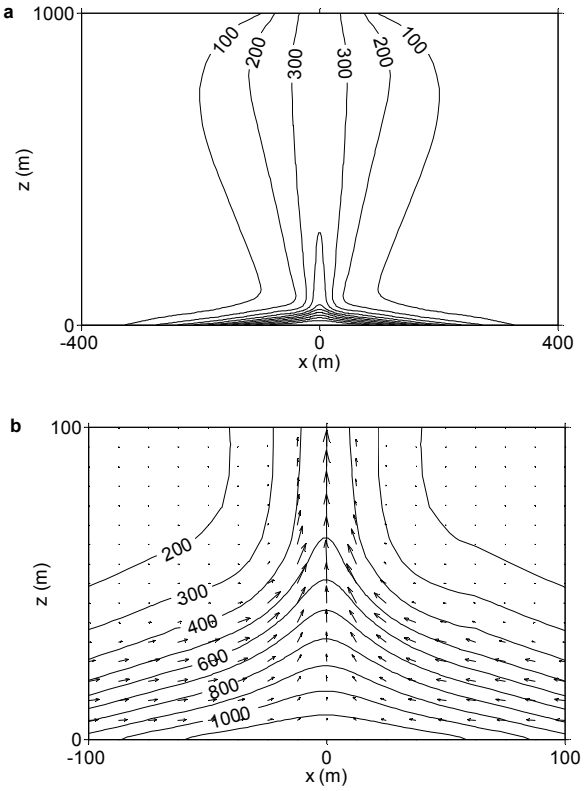

Figure 1 The steady state temperature distribution in a convection cell at seafloor pressures. The top boundary (z=1000 m) represents the seafloor and is permeable. Here, the pressure is held at 25 MPa (equivalent to ~2.5 km below sea surface). The temperature boundary condition is T=10°C where flow is downwards, and $\partial T/\partial z$=0 where flow is upwards. The side boundaries for the simulation are at x=-1700 m and x=1700 m (beyond the range of these figures), sufficiently distant that they do not influence the solution near the heater. They are held at T=10°C and cold hydrostatic pressure. The bottom boundary (z=0) is impermeable. A Gaussian (bell-shape) temperature profile is imposed, representing a magma chamber. The temperature on z=0 runs from 'cold' (10°C) at the sides to 'hot' (1200°C) in the centre. Parameters for the simulation are porosity=10%, permeability k=10^{-14} m^2, thermal conductivity λ=2.0 $Wm^{-1}K^{-1}$. **a**, The overall temperature structure of the convection cell, showing the distinction between the boundary layer and the plume. Isotherms from 100°C to

1100°C are drawn, in increments of 100°C. Flow vectors are omitted for clarity. Flow is downwards at the sides, towards the centre at the base and upwards in the centre. **b**, A close-up view of the flow regime and temperature structure inside the boundary layer, showing the bottom 100 m of the domain. Isotherms from 200°C to 1100°C are drawn, in increments of 100°C. Vectors are of Darcy velocity.

[figure 1 is 31% original size **]**

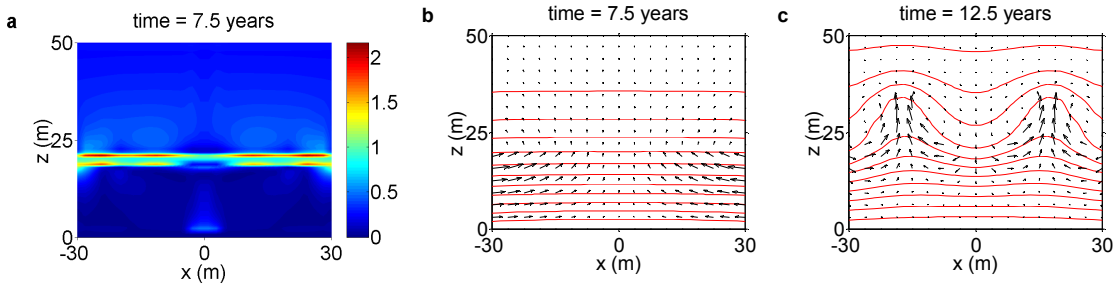

Figure 2 Figures showing the early stages of the simulation, at the bottom of the domain shown in figure 1. **a**, Colour plot of the local Rayleigh number Ra_L, before plume formation. The regions of greatest Ra_L indicate where plumes are likely to form. **b**, The temperature and flow fields before plume formation. The thermal structure is governed by conduction alone. Convective motion exists, but it does not influence the temperature field. **c**, The temperature and flow fields after plume formation. Advection has begun to distort the thermal structure. (As the simulation progresses to steady state, these two plumes coalesce to form the single plume in figure 1). Isotherms are drawn from 100°C (top) to 1100°C (bottom) in increments of 100°C. Vectors are of Darcy velocity.

[figure 2 is 22% original size **]**

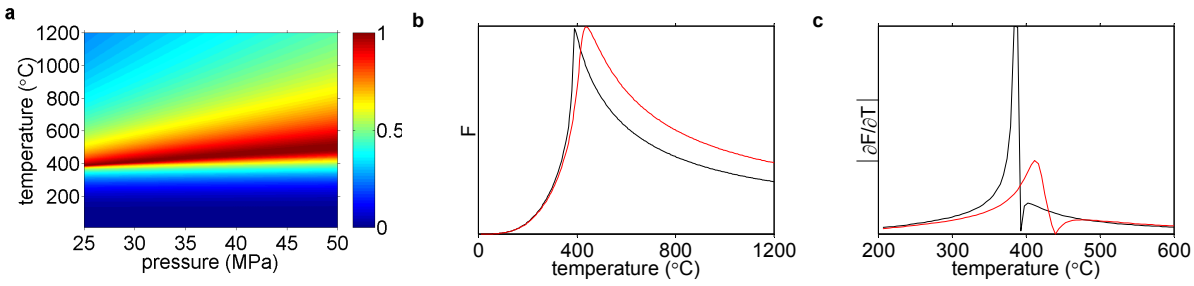

Figure 3 a, 'Fluxibility' F (in normalised units) as a function of temperature T and pressure p. The pressure range of 25 MPa to 50 MPa (~2.5 km to ~5 km cold hydrostatic head) is representative of the pressures found in seafloor hydrothermal systems. **b**, F (in normalised units) plotted against T at p=25 MPa (black line) and p=35 MPa (red line). These pressures are lower and upper bounds for the pressures to be found in the cell in fig.1. **c**, $\left|\partial F/\partial T\right|$ (in normalised units) plotted against T at p=25 MPa (black line) and p=35 MPa (red line). The temperature at which $\left|\partial F/\partial T\right|$ is maximised is, approximately, the temperature at which plumes form.

[figure 3 is 22% original size **]**